Molecular Dynamics Simulation of Cytochrome b_5: Implications for Protein−Protein Recognition†

Elizabeth M. Storch and Valerie Daggett*

Department of Medicinal Chemistry, University of Washington, Seattle, Washington 98195-7610

Received February 20, 1995; Revised Manuscript Received May 12, 1995®

ABSTRACT: Cytochrome b_5 participates in electron-transfer reactions with a variety of different proteins. To explore how this protein might discern between structurally varied proteins, we have performed a molecular dynamics simulation focusing on its structural stability and dynamic behavior in solution. The protein was simulated in water at 298 K and pH 6.9 for 2.5 ns. The protein deviated significantly from the crystal structure midway through the simulation, but ultimately the crystalline conformation was regained. The simulation was at all times well behaved as judged by comparison to structural NMR data obtained in solution. One region of the protein backbone that deviated from the crystal conformation contains acidic residues implicated in electrostatic-based protein−protein recognition. The mobility in this region caused the protein to display different patterns of residues at the surface with time, as well as the formation of a large cleft partially exposing the hydrophobic core lining the heme pocket. Furthermore, the position and cyclical formation of this cleft suggest that hydrophobic interactions may be important in protein−protein recognition events and possibly even electron transfer, as the cleft allows for easy access to the heme group. These results indicate that thermal motion could provide a low-energy mechanism for controlling recognition events. Thus, the dynamical behavior observed through the varying solution conformations sampled may be important in influencing the diverse range of protein−protein interactions in which cytochrome b_5 participates.

The link between protein structure and function relies heavily on the detailed information provided by high-resolution X-ray crystallography experiments. This information allows direct visualization of the structure of a protein and may reveal details of biological relevance. Motion, however, is implicated in biological function, and the crystal structure of a protein represents an average conformation. Some or all of the residues may have a variety of preferred conformations that would not be captured in a single static depiction (Smith et al., 1986). In addition, studies have also revealed that structures of proteins (or portions of a protein) in solution and in a crystalline environment can be quite different [e.g., Clore et al. (1987), Housset et al. (1991), Hua and Weiss (1990), Kline et al. (1988), Pflugrath et al. (1986), Urbanova et al. (1991), Weiss et al. (1989), and Wittekind et al. (1992)]. Proteins exhibit a variety of complex motions even in their resting states. The magnitude of the motion experienced by the protein can increase dramatically during binding, catalytic, and signal transduction events. A recent study suggests that normal room temperature movements of proteins in solution can span up to ~15 Å (Careaga & Falke, 1992). The picture is complicated further in light of Frauenfelder and co-workers' suggestions that native proteins can occupy numerous distinct conformational substates that perform the same function but at different rates and that thermal energy and environmental conditions determine which of these states is preferred (Hong et al., 1990).

Experimental studies generally only yield limited amounts of information of the actual molecular details of the motion experienced by a protein. Molecular dynamics simulations provide a way of analyzing motion at the atomic level as a function of time and of obtaining a physical description of protein behavior. Through such simulations, the motions that are inferred by nuclear magnetic resonance (NMR) relaxation and crystalline *B*-factors can be investigated. Hence, the simulations should be consistent with the physical picture provided by NMR and crystallography. To date, few studies have compared molecular dynamics generated structures with both crystallographic and structural NMR data, mostly because solution NMR structures are rarely available. Braatz et al. (1992) made such comparisons for a long simulation (3 ns) of the protein ubiquitin; however, explicit solvent molecules were not included. The properties of interleukin-1β were investigated in a 550 ps simulation by Chandrasekhar et al. (1992). Only a thin shell of waters was added to solvate this protein, but good agreement with experiment was achieved. Brunne et al. (1993) have described a long simulation (1.4 ns) of bovine pancreatic trypsin inhibitor, which proved to be in good agreement with experiment. Recently, Li and Daggett (1995) made direct comparison between structures determined using X-ray crystallography and 2-D NMR and those generated during a 5.3 ns molecular dynamics simulation of chymotrypsin inhibitor 2 in solution. However, there is still a need to make further comparisons for other systems employing a large number of water molecules and reaching the nanosecond regime to ensure that the simulated structures adequately reflect the structural and dynamical properties of proteins in solution. Cytochrome b_5 is a good system to study with molecular dynamics techniques. The protein is small (85

† This research was supported by start-up funds from the Department of Medicinal Chemistry.

* To whom correspondence should be addressed [Fax, (206) 685-3252; E-mail, daggett@fitz.mchem.washington.edu].

® Abstract published in *Advance ACS Abstracts,* July 1, 1995.

0006-2960/95/0434-9682$09.00/0

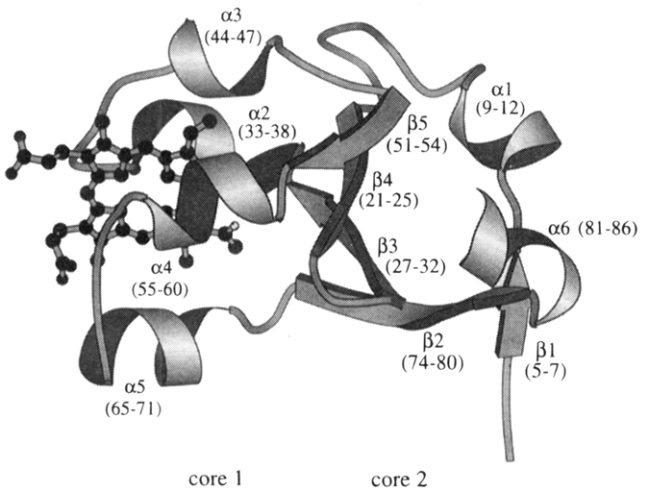

FIGURE 1: Ribbon diagram of the crystal structure of cytochrome b_5 including the prosthetic heme group (Mathews et al., 1972). The residues involved in the secondary structure are given in parentheses. The bovine numbering scheme is used. This figure was constructed using the Molscript program (Kraulis, 1991).

residues), a high-resolution crystal structure is available (1.5 Å; Mathews et al., 1972), and the solution structure has been characterized by 2-D NMR techniques (Guiles et al., 1990, 1992; Lecomte & Moore, 1991; Moore & Lecomte, 1990; Moore et al., 1991; Veitch et al., 1988).

Cytochrome b_5 is a low-spin hemoprotein that exists in several forms and plays a role as an electron-transfer mediator in a variety of redox systems (Mathews & Czerwinski, 1976). Of particular interest is its involvement in the drug metabolizing P450-dependent reactions where it transfers the second electron necessary for substrate oxidation (Schenkman & Greim, 1993). One naturally occurring soluble form and two membrane-bound forms of the protein exist. The soluble form is found in erythrocytes, and its role is to reduce methemoglobin (Hegesh et al., 1986). The physiological role of the membrane-bound mitochondrial form is unknown (Lederer et al., 1983; Strittmatter & Velick, 1956). A water-soluble form of the hepatically bound cytochrome b_5 can be released by lipase or proteolytic solubilization. This fragment contains the heme and retains activity with respect to protein recognition and electron transfer. The structure of the lipase-solubilized bovine liver cytochrome b_5 has been determined by X-ray crystallography (Mathews et al., 1972) and is used as the starting point for our work.

The structure of hepatic cytochrome b_5 consists of a heme-containing region and a hydrophobic tail that anchors the protein to the endoplasmic reticulum. The soluble portion is composed of six α-helices, five strands arranged in a β-sheet, and several β-turns (Figure 1). A prosthetic heme group located in the crevice formed by four of the helices (α2−α5) is partially accessible to the solvent and is coordinated to His 39 and His 63. The crevice is lined with nonpolar residues and constitutes hydrophobic core 1 (Figure 1). Another hydrophobic core (core 2) is located on the opposite side of the protein. This core appears to be important in maintaining the structural integrity of the protein (Mathews et al., 1979). It is also an independent structural domain during folding (Moore et al., 1991; Moore & Lecomte, 1993). The results of 2-D NMR experiments suggest that the solution structure of cytochrome b_5 closely resembles the crystalline structure, although the protein is more dynamic in solution (Guiles et al., 1990, 1992).

Extensive experimental data are available regarding the structural properties of cytochrome b_5 and the potential recognition sites for its interactions with other proteins. The details surrounding macromolecular recognition began to emerge with the computer-generated models of cytochrome b_5 complexed with other proteins. These models focused on protein−protein interactions based on complementary charge pairing at the interface of the complex. An array of acidic residues surrounding the partially buried heme group of cytochrome b_5 was proposed to participate in the formation of cytochrome b_5−cytochrome c complexes (Mauk et al., 1986; Salemme, 1976; Wendoloski et al., 1987). Models of cytochrome b_5 complexed with methemoglobin (Poulos & Mauk, 1983), metmyoglobin (Livingston et al., 1985), and cytochrome P-450$_{cam}$ (Stayton et al., 1989) implicated the same or neighboring acidic residues. Using chemical modification, protection experiments, and site-directed mutagenesis studies, the results of the computer models have been largely substantiated (Mauk & Mauk, 1989; Ng et al., 1977; Rodgers et al., 1988; Rodgers & Sligar 1991; Strittmatter et al., 1990; Tamburini et al., 1985).

Initially we performed the simulation described here as a control for simulation studies of the apo form of the protein, which adopts a partially folded conformation that appears to be an intermediate along the folding pathway (E. M. Storch and V. Daggett, manuscript in preparation). However, the behavior of the native holo form was unexpected, and we became interested in the structural and dynamical characteristics of cytochrome b_5 and their possible relation to macromolecular recognition. To this end, the protein was simulated in water at 298 K and pH 6.9 for 2.5 ns. This time scale revealed macroscopic conformational changes that would not have been detected in a shorter simulation. The mobility of the protein was mainly localized to two regions and resulted in conformations displaying different patterns of residues on the surface, as well as the periodic formation of a large cleft. The dynamic behavior of cytochrome b_5 observed may be important in influencing the diverse range of protein−protein interactions in which this protein participates.

METHODS

The starting conformation of cytochrome b_5 was obtained from the Brookhaven Protein Data Bank (PDB Accession Number 3b5c). The structure was determined by Mathews et al. (1972) to 1.5 Å resolution. The solubilized form of oxidized, bovine liver cytochrome b_5 contains 93 residues. Residues 1−2 and 88−93 were not visible in the electron density maps and were therefore omitted in our starting structure for the simulation. The potential energy function (Levitt, 1983, 1989; Levitt et al., 1995a,b) and associated protocols (Daggett & Levitt, 1992) are described in detail elsewhere. The heme parameters of Henry et al. (1985) were used. Energy minimization and molecular dynamics were performed using the program ENCAD (Levitt, 1990) on a Silicon Graphics Iris Indigo computer. All atoms were present in the simulation, and the system was modeled to mimic an experimental pH of 6.9 (i.e., Lys, Arg, and His 15 were positively charged; His 26 and His 80 were neutral; and Glu and Asp were negatively charged). The experi-

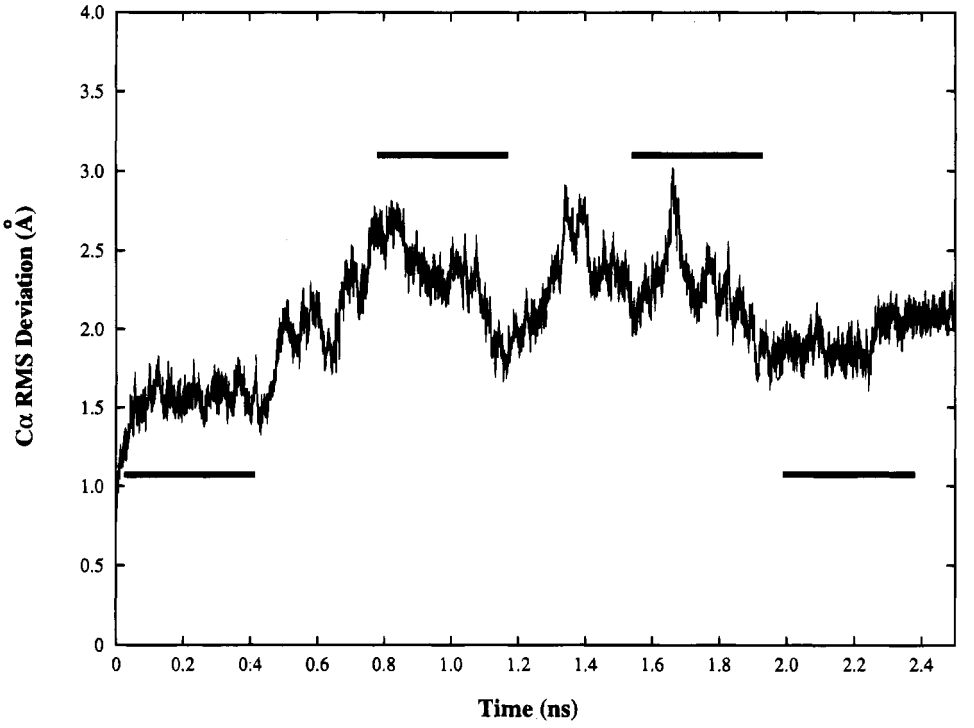

FIGURE 2: C_α RMS deviation from the crystal structure as a function of time. Large deviations from the crystal structure were observed, and the crystal conformation was recovered. Four main regions of the trajectory were analyzed and are indicated by the horizontal bars. The C_α RMS deviation was calculated after optimum superposition of the protein coordinates (Kabsch, 1976).

mentally determined pK_a values were used in assigning the ionization state of the His residues (Altman et al., 1989). The system consisted of the protein in a rectangular box of water molecules, with walls at least 8.0 Å from any protein atom (3034 water molecules). The water density was set to the experimental value (0.997 g/mL) for 298 K (Kell, 1967) by adjusting the volume of the box.

Initially, conjugate gradient minimization of the protein was carried out for 2000 steps in order to reduce unfavorable contacts. The water molecules were then added, and the water only was minimized for 2000 steps, followed by 2000 steps of molecular dynamics and another 2000 steps of minimization. The protein was subsequently minimized for 2000 steps followed by minimization of the entire system for 2000 steps. After the preparation, the atoms were assigned velocities according to a Maxwellian distribution. The system was brought to the target temperature by adjusting the velocities intermittently until the system reached the desired temperature of 298 K, which occurred in 2−3 ps. After this point, the total energy was constant and no further scaling of velocities was necessary. Periodic boundary conditions were employed, and the box volume was held constant during the simulation. Molecular dynamics was performed for 1.25×10^6 steps utilizing a 2 fs time step, resulting in a 2.5 ns trajectory. Structures were saved every 0.2 ps for further analysis (12 500 structures). An 8.0 Å nonbonded cutoff was used, and the nonbonded list was updated every five steps.

RESULTS

Overall Structure. The C_α root mean square (RMS) deviation from the crystal structure as a function of time is shown in Figure 2. The deviation ranged from 1.3 to 3.0 Å, excluding the first 0.2 ns (200 ps). The first 0.2 ns reflected an equilibration period for the system. The initial 0.5 ns and last 0.6 ns displayed similar average deviations from the crystal structure, approximately 1.5 and 1.8 Å, respectively. The 0.6−1.9 ns segment showed more dramatic fluctuations. These different segments of the trajectory were chosen for further study and are marked in Figure 2.

The deviation from the crystal structure was not distributed uniformly throughout the protein (Figure 3). Instead, the mobility was localized to approximately three regions, residues 10−20 (region 1), 40−52 (region 2), and 65−75 (region 3), which comprise a loop, α3 and adjacent loops, and α5/β2, respectively (Figure 1). For short periods of time, the C_α RMS deviation from the crystal structure in these regions reached distances of >5.0 Å. Region 1 experienced large-scale RMS deviations from 1.2 to 1.55 ns. Region 2 deviated from the crystal structure for the duration of the simulation after 0.5 ns. Region 3 fluctuated from 0 to 1.75 ns and then returned to the conformation observed in the crystal structure.

Internal Motion. The C_α RMS fluctuations describing the motion about the mean structure were used to determine the distribution of mobility along the sequence as a function of time. The RMS fluctuation for the first 0.4 ns was approximately 0.8 Å. This constancy paralleled the RMS deviation from the crystal structure (Figure 2). Throughout the course of the simulation, large RMS fluctuations were localized to the three main regions of the protein described above. Residues 10−20 reached peak fluctuations of 1.5 Å. The RMS fluctuation of residues 40−52 oscillated between 1.0 to 2.0 Å. The C-terminus (residues 83−86) displayed similar large-scale oscillations. Residues 65−75 remained relatively constant, except from 1.6 to 2.0 ns. During the last 0.1 ns, the RMS fluctuation for all residues, excluding the C-terminus, remained below 0.8 Å and

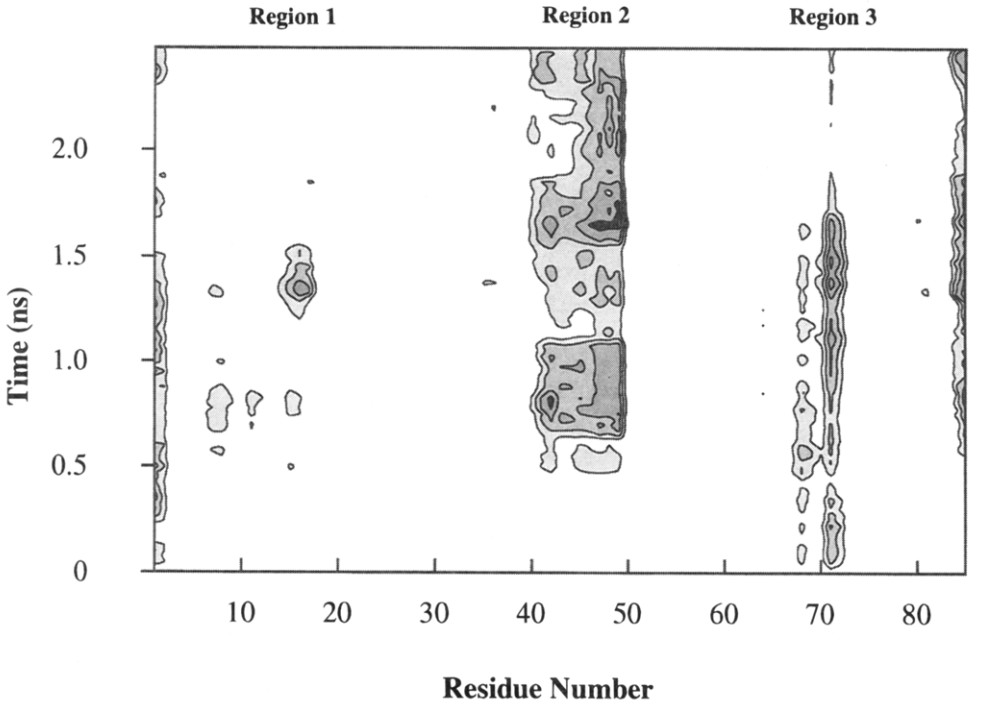

FIGURE 3: Contour plot of the C_α RMS deviation per residue number as a function of time. Deviations are outlined as follows: ≤3.0 Å white; 3.0 Å ≤ light gray ≤ 4.0 Å; 4.0 Å ≤ gray ≤ 5.0 Å; 5.0 Å ≤ dark gray ≤ 6.0 Å; and ≥6.0 Å black. The three regions of high deviation discussed in the text are labeled.

paralleled the evenness of the RMS deviation from the crystal structure (Figure 2).

Overall, the C_α fluctuation for the crystal structure is ~0.6 Å as estimated from the experimental *B*-factors using the following relationship: C_α fluc $= (3B/8\pi^2)^{1/2}$, which assumes that all motion is internal and that the contribution from lattice disorder is negligible. The corresponding values from the last 0.5 ns of the simulation are displayed in Figure 4 for comparison. While the positions of relative mobility are similar (graphics portion of Figure 4), the magnitude of the motion in the solution simulation differs from the crystal structure (plot in Figure 4). For the three main regions described above and marked in Figure 4, the first two show increased motion in both environments. Region 2 is particularly prominent in the simulation, and although relatively mobile in the crystal structure, this portion of the protein appears to be involved in crystal contacts (plate I; Mathews et al., 1972), which may hinder its mobility. Region 3 also appears to be involved in crystal contacts and shows low mobility in the crystal structure. Interestingly, the portions of the protein exhibiting low mobility in the simulation have lower fluctuations than those estimated from the *B*-factors (by ~0.2 Å), which may indicate the magnitude of the contribution of the lattice disorder. Additionally, the relative number of intraprotein contacts in these regions, although shifted to the right slightly, is higher than in mobile regions (bar graph, Figure 4).

Secondary Structure. To determine the origins of the localized mobility detected through the C_α RMS fluctuations and displayed in the main-chain traces, we investigated how the helical and β-content changed with time (Table 1). The method used to determine the secondary structure is based on repeating segments of at least three residues in succession containing either helical or β-structure, as indicated by (ϕ,ψ) dihedral angles (Daggett et al., 1991; Daggett & Levitt, 1992). The four time periods were chosen to represent the prominent regions of the plot in Figure 2: the beginning (0−0.4 ns), the two fluctuating periods (0.6−1.0 and 1.4−1.8 ns), and the end (2.0−2.4 ns).

Table 1: Secondary Structure Content for Particular Regions of Cytochrome b_5 as a Function of Time[a]

secondary structure[b]	crystal structure	time (ns)			
		0−0.4	0.6−1.0	1.4−1.8	2.0−2.4
α1 (9−12)	100	87 (33)	84 (37)	82 (38)	81 (39)
α2 (33−38)	33	32 (24)	64 (29)	55 (29)	47 (30)
α3 (44−47)	100	96 (18)	92 (24)	93 (20)	98 (11)
α4 (55−60)	100	98 (7)	98 (7)	99 (6)	98 (8)
α5 (65−71)	100	85 (11)	81 (14)	85 (12)	83 (11)
α6 (81−86)	83	31 (31)	10 (15)	9 (19)	24 (27)
β1 (5−7)	100	97 (16)	97 (18)	97 (17)	97 (15)
β2 (74−80)	57	20 (23)	14 (20)	10 (19)	13 (19)
β3 (27−32)	67	58 (15)	66 (2)	66 (4)	67 (1)
β4 (21−25)	100	83 (32)	84 (20)	88 (19)	99 (6)
β5 (51−54)	0	0	0	0	0

[a] α-Helical or β-structure is defined as having at least three consecutive residues with the appropriate (ϕ,ψ) dihedral angles (Daggett & Levitt, 1992). Secondary structure contents are given in percentages, so, for example, 33% of the residues in α2 adopt helical (ϕ,ψ) angles in the crystal structure. The values from the simulation are averages over particular regions of the sequence, as specified, and the time interval. The standard deviation is given in parentheses alongside each value. [b] The elements of secondary structure are shown in Figure 1, and the residue numbers are given in parentheses.

α1 showed a constant average helical content but experienced large fluctuations with time (note that a 30% standard deviation for this segment corresponds to one residue out of three). α2 exhibited the largest change in helical content during the course of the simulation. During the first 0.4 ns, α2 contained the same helical content as the crystal structure, and the helix content increased 2-fold during the two fluctuating time periods (0.6−1.0 and 1.4−1.8 ns). The dramatic change in helix content of α2 for each time period, coupled with the large standard deviations, indicated that this segment was conformationally heterogeneous. It

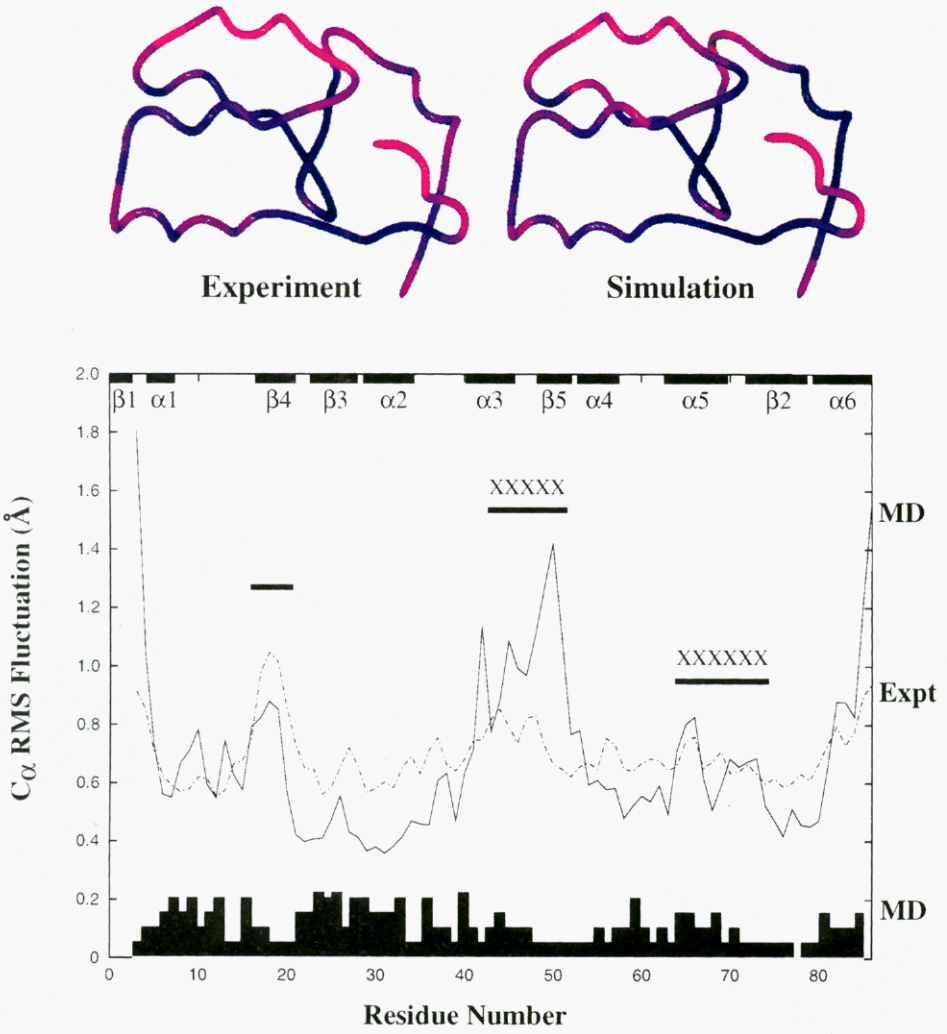

FIGURE 4: (Top) Main-chain C_α traces of cytochrome b_5 depicting the relative mobility as determined from the experimental *B*-factors (see text) and the C_α RMS fluctuation from the last 0.50 ns of the simulation. Structures are colored according to relative motion from blue (low mobility) to red (high mobility). (Bottom) The C_α RMS fluctuation as a function of residue number, where experiment is shown with the dashed line and simulation with the solid line. The observed crystal contacts (plate I; Mathews et al., 1972) are indicated with XXX. The relative number of intraprotein contacts (atoms ≤4.5 Å) during the simulation, not including contacts within or between neighboring residues, is indicated by the bar graph at the bottom of the plot. The bar graph is normalized so that 0.2 equals the maximum number (250) of average contacts a residue makes during MD.

should be noted that, because of its irregular nature, α2 is defined as a series of turns by Mathews et al. (1972). In contrast, α4 and α5 maintained stable helical structure throughout the simulation. α6 consistently remained below 50%, reaching low points of 0% from 0.7 to 1.0 ns and from 1.2 to 1.6 ns. These residues make up the carboxy terminus, which is less constrained than other regions of the protein.

The $i \rightarrow i + 4$ hydrogen bonds for all six helices were analyzed as another measure of the secondary structure, where a hydrogen bond was defined as having a distance between a carbonyl oxygen atom and an amide hydrogen atom of ≤2.6 Å and with a hydrogen-bonding (N−H···O) angle within 45° of linearity. All of the helices maintained α-helical hydrogen bonding throughout the simulation with the exception of α6 at the carboxy terminus, whose hydrogen-bonding pairs fluctuated about 3.2 Å (data not shown). Even though α2 showed large fluctuations based on repeating structure (Table 1), the $i \rightarrow i + 4$ hydrogen bonds were maintained throughout the simulation. In addition, α3 and α4 also showed increased motion (Figure 4) but maintained ideal α-helical hydrogen-bonding patterns.

Among the β-strands, β2 deviated the most from the crystal structure. β2 contained a decreased β-content of less than 20% during the simulation. The first few residues of this region also displayed an increased C_α RMS fluctuation relative to other residues in the protein, as mentioned previously. β5 never contained β-content according to our definition of repeating structure in either the simulation or crystal structure. The beginning portion of β5 contained residues that also displayed large fluctuations. Both β2 and β5 are defined as irregular in the Brookhaven PDB file. The involvement of β2 and β5 in the β-sheet will be justified below through NOE connectivities.

NOE Connectivities. Interresidue hydrogen−hydrogen distances were also monitored to compare with experimentally observed nuclear Overhauser enhancement (NOE) connectivities. The predicted NOEs from the simulation were obtained by calculating an average weighted distance ($r_w = \langle r^{-6} \rangle^{-1/6}$) between the interacting hydrogens. All of the hydrogen−hydrogen distances corresponding to the experimentally observed NOEs in the β-sheet (Guiles et al., 1990; Moore & Lecomte, 1993) remained below 5.0 Å, which is considered a reasonable cutoff for an NOE (Wüthrich, 1986), throughout the simulation except for the

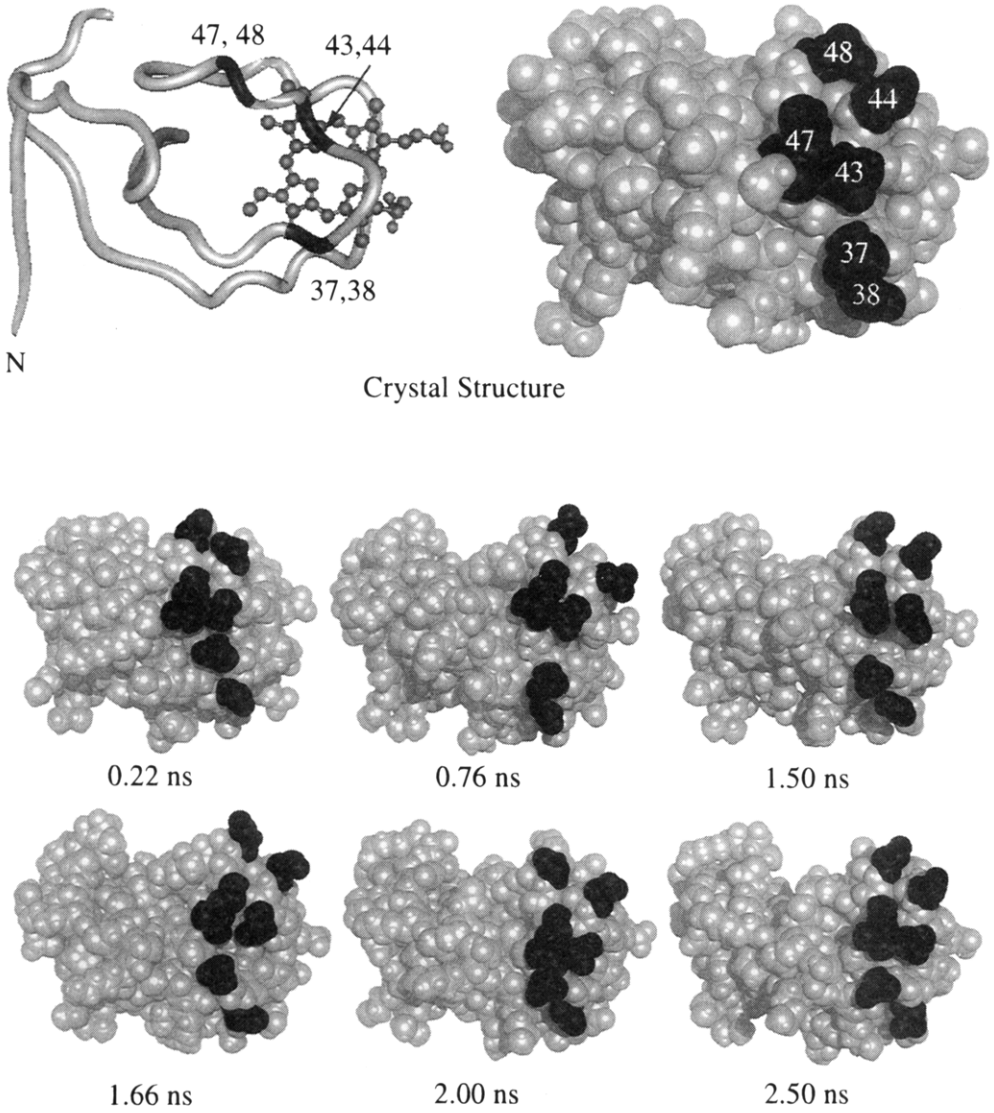

FIGURE 5: Main-chain trace and space-filling representations of the crystal structure and snapshots from the simulation of cytochrome b_5. Residues Glu 37, Glu 38, Glu 43, Glu 44, Arg 47, and Glu 48 are depicted in black. The different snapshots highlight the distinct surfaces that were displayed during the simulation.

$d_{\alpha N}$ connectivities between 23−51 and 23−52. Maximum average distances of 7.6 and 6.8 Å, respectively, were observed for these interactions during the 1.6−1.8 ns time segment, where the values were below 5.0 Å prior to this. Even though these large interresidue distances occurred, the native-like structure was reestablished in the latter part of the simulation, and the distances dropped back below 5.0 Å. The connectivities observed in the α-helical regions were also monitored ($d_{\alpha N(i+3)}$) (Guiles et al., 1990, 1992). All of the appropriate proton pairs remained below 5.0 Å during the simulation (data not shown). In addition, the NOEs between Tyr 30 and Phe 74, forming the connectivities between β3 and β2 at the back wall of the heme pocket, were also observed (Moore & Lecomte, 1990; Reid et al., 1987).

In addition to the main-chain NOEs within secondary structure described above, side-chain NOEs between residues located mainly within core 2 have been determined (Moore & Lecomte, 1990). All hydrogen−hydrogen distances for these core NOEs remained below 5.0 Å, thus demonstrating the integrity of the hydrophobic core. NOEs between the side chains of residues 26 and 55 (Moore & Lecomte, 1993; Reid et al., 1987), representing the interface of the cores, remained ≤4.0 Å during the simulation. Furthermore, although the N-terminus was structurally labile, α6 remained docked to β1 as monitored through the observed d_{NN} NOE connectivities between residues 7−78 and 7−80 (Moore & Lecomte, 1993).

Protein Surface. As discussed above with reference to Figure 3 and the C_α RMS fluctuations, three distinct regions of the protein showed high mobility. Region 2 (residues 40−52) comprises α3 and the loop following it (Figure 1). Residues in this region occupy the periphery of one side of the heme pocket and are predominantly acidic. The high percentage of acidic residues in cytochrome b_5, 11 glutamates and 6 aspartates, made assignment of the side-chain conformations in this region by 2-D NMR nearly impossible (Guiles et al., 1990). Space-filling representations highlighting some of these acidic residues (Glu 37, Glu 38, Glu 43, Glu 44, and Glu 48) and Arg 47, which is involved in a salt bridge (Veitch et al., 1990), illustrate that distinct surfaces were displayed at different time points during the simulation (Figure 5, the orientation of the protein has been changed to better illustrate the surface of interest).

The charged residues initially occurred as three groups in the crystal structure: Glu 44/Glu 48, Glu 43/Arg 47, and

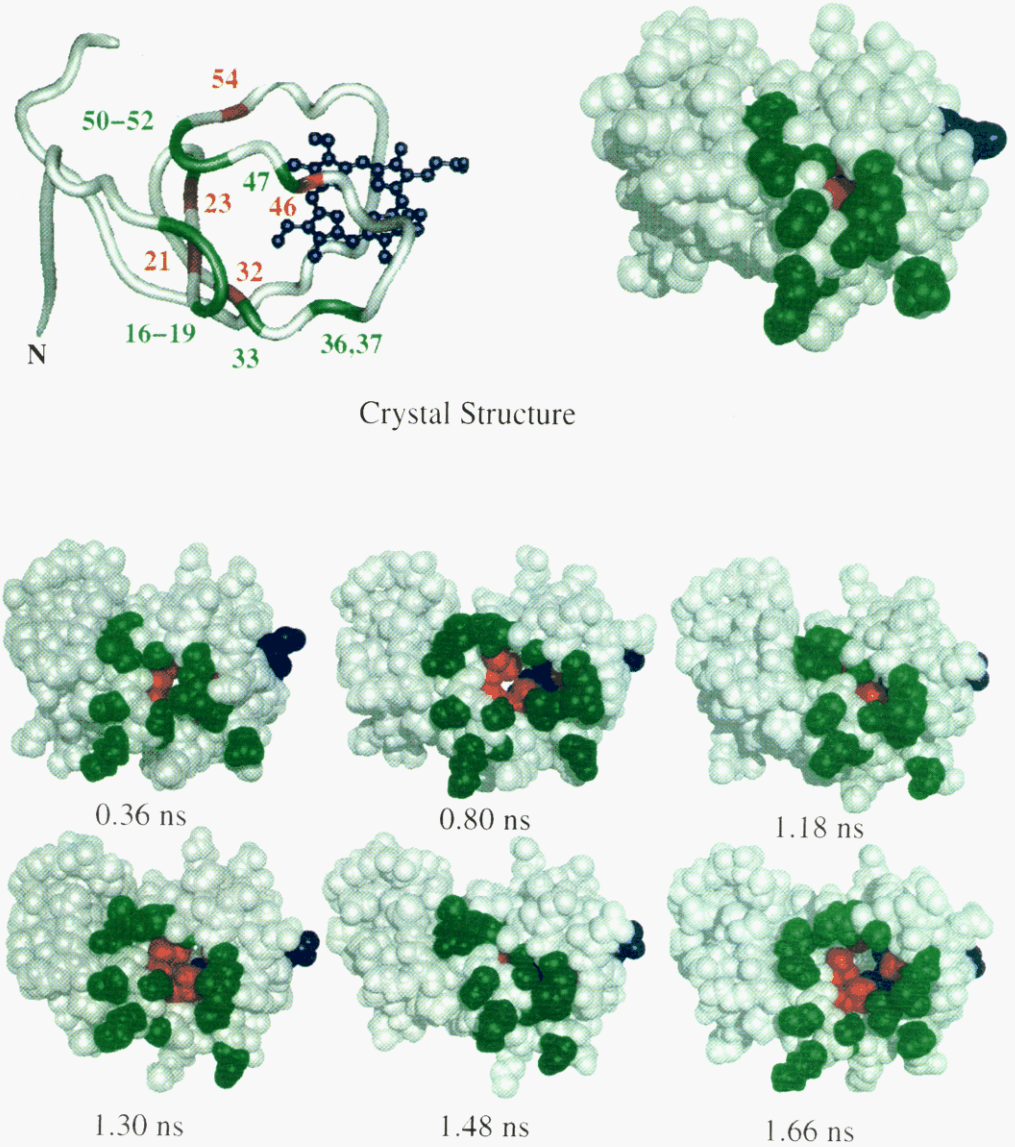

FIGURE 6: Main-chain trace and space-filling representations of cytochrome b_5. The buried residues that intermittently became exposed upon cleft formation (Thr 21, Leu 23, Leu 32, Leu 46, and Ala 54) are colored red. The residues in green (Asn 16, Asn 17, Ser 18, Lys 19, Ile 24, Thr 33, Leu 36, Glu 37, Arg 47, Ala 50, Gly 51, and Gly 52) depict surface residues along the rim of the cleft. The prosthetic heme group is colored blue.

Glu 37/Glu 38. Glu 44 and Glu 48 ultimately moved apart during the simulation as compared to the crystal structure, where they are nestled next to each other (Figure 5). The distances between the ϵ-amino hydrogen of Arg 47 and the carboxylate oxygen of Glu 43 and Glu 37 were monitored during the simulation as a probe of the surface changes. At approximately 1.4 ns, the salt bridge present in the crystal structure between Glu 43 and Arg 47 (2.4 Å) broke but reformed by 1.8 ns (~3.4 Å). Glu 37 and Glu 38 fluctuated greatly during the simulation: at 1.7 ns, they were separated by a distance of ~12.0 Å, as compared to 6.0 Å in the crystal structure. By 1.8 ns, Glu 37 also formed a salt bridge with Arg 47, with an average distance of 1.6 Å. Throughout the simulation, all of the residues remained exposed on the surface of the protein.

Regions 1 (residues 10−20) and 2 (residues 40−52) are also depicted through space-filling representations in Figure 6 (same orientation as Figure 5). Various structures from the simulation illustrate that the movement of these regions alternately exposed and buried a hydrophobic core, comprised of Thr 21, Leu 23, Leu 32, Leu 46, and Ala 54 (Figure 6). The opening and closing of the cleft occurred in intervals of 0.3−0.6 ns. The maximum dimensions of the cleft were 15.2 Å × 10.5 Å × 11.5 Å (length by width by depth), and the corresponding dimensions in the crystal structure are 16.5 Å × 4.7 Å × 5.7 Å.

The solvent-accessible surface area of the residues in the cleft is given in Table 2. All of the residues are completely buried in the crystal structure and gain varying degrees of exposure during the simulation. Early on, all residues except for Ala 54 became accessible to solvent. Thr 21 became buried from 1.15 to 1.5 ns, which correlated with the opening of the cleft, as observed through the snapshots (0.80 and 1.48 ns) in Figure 6. Leu 23 remained buried from 0.45 to 1.6 ns and is located just behind Thr 21 in Figure 6. Leu 32 was alternately buried and exposed during the simulation. Leu 46, located on the other side of the cleft relative to the aforementioned residues (Figure 6), was exposed to solvent early on but later became buried. At 1.6 ns all of the residues had large positive changes in their solvent-accessible surface area that lasted for approximately 0.3 ns. This dramatic opening of the cleft is illustrated in the 1.66 ns snapshot

Table 2: Change in Solvent-Exposed Surface Area of Residues Located in the Cleft[a]

	time (ns)							
residue	0.2−0.25	0.5−0.55	0.8−0.85	1.1−1.15	1.4−1.45	1.7−1.75	2.0−2.05	2.3−2.35
Thr 21	21	25	30	10	6	15	11	10
Leu 23	27	12	15	8	3	21	7	10
Leu 32	57	10	22	8	12	18	4	8
Leu 46	13	18	9	12	7	37	11	6
Ala 54	2	6	8	6	3	7	11	13

[a] The values shown are in Å^2. The average change in solvent accessible surface area (Lee & Richards, 1971) is given over the averaging interval indicated. All of the changes are relative to the accessible surface area of residues in the crystal structure, which was 0 Å^2 for all residues.

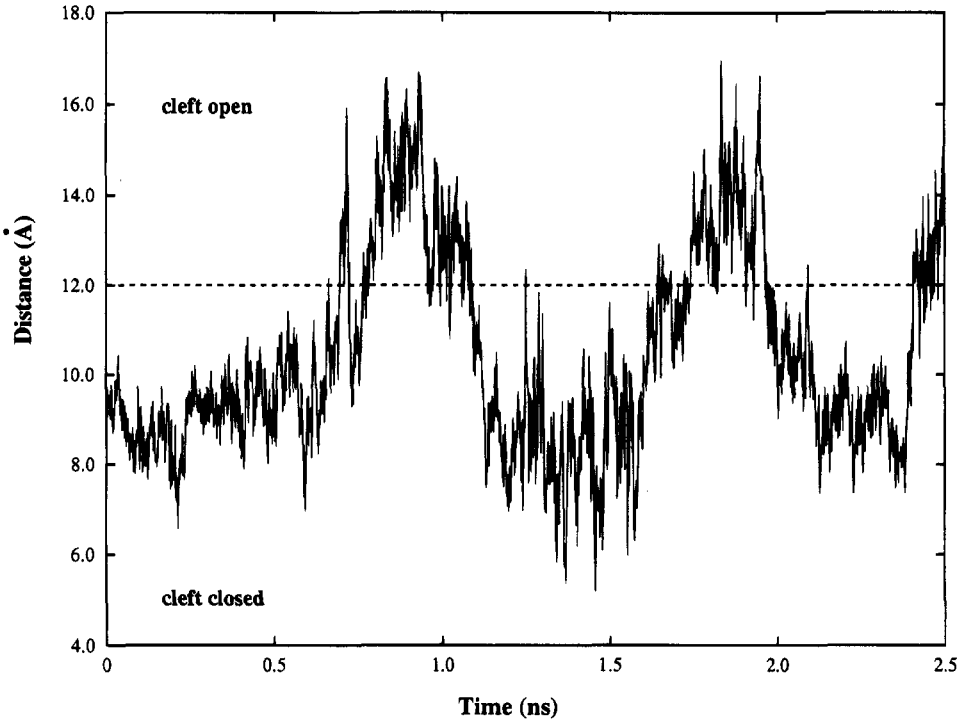

FIGURE 7: Distance between Ser 18 and Ala 50 as a function of time. Distances were measured from the hydroxyl hydrogen of Ser 18 to a methyl hydrogen of Ala 50. These two residues define partial boundaries of the cleft. The starting distance in the crystal structure was 9.4 Å. Distances below the dashed line indicate that the cleft was closed and above 12.0 Å the cleft was open.

(Figure 6). From this open position, it is evident that this cleft allows access to the heme group (note the atoms of the heme in blue at the bottom of the cleft in the 0.80 and 1.66 ns structures of Figure 6). From 1.9 ns until almost the end of the simulation, all of the residues except Ala 54 became buried. Ala 54 is located away from the other residues and displayed a different pattern of exposure (Table 2).

The distance between Ser 18 and Ala 50, two residues that span the rim of the cleft, correlated with the opening and closing of the two regions (Figure 7). These distances reflect the solvent accessibility of the internal hydrophobic residues. Distances during the simulation ranged from 4.8 to 17.5 Å, as compared to the crystal structure value of 9.4 Å. The change of distance from low to high values parallels the opening and closing of the cleft as observed in the space-filling representations in Figure 6. At the end of the simulation, the distances between Ser 18 and Ala 50 began to rise again, suggesting the beginning of another cyclical opening of the cleft.

DISCUSSION

Molecular dynamic simulations are now frequently utilized to help elucidate the link between protein structure, mobility, and function. During the process of reaching this ultimate goal, several research objectives must be met. In this regard, our main objective was to perform a molecular dynamics simulation of cytochrome b_5 in a native environment and determine the stability of such a system over a long time period. Furthermore, we wanted to know what length of time would be needed in order for the structural implications from the simulation to be physically relevant. A great deal of predictive power still relies on the crystal structures of proteins. Therefore, we also set out to assess how our simulation compares to the crystal structure of cytochrome b_5 and also whether the simulation accurately models the solution structure and behavior of cytochrome b_5. In the course of investigating these issues, interesting surface properties of the protein became apparent. Below we first discuss the stability of the simulation and then the possible biological relevance of the observed motion.

A gross overview of the simulation is provided by the C_α RMS deviation plot (Figure 2). The 2.5 ns length of the simulation allows the molecule to explore different conformations that would not have been possible in a single shorter simulation. As a whole, the molecule adopted solution conformations that varied from the crystal structure, yet returned to a state that closely resembled the starting conformation. The secondary structure content (Table 1) and

hydrogen−hydrogen distances corresponding to NOEs reflected the stability of the simulation, as well. On the basis of secondary structure content, the entire protein was well behaved with minor exceptions involving α1, α2, α6, β2, and β5. α1 and α2 however, did maintain proper α-helical hydrogen bond distances, while β2 participated in all of the experimentally observed interactions with β1 and β3. Moore and Lecomte (1993) found that the β-sheet and the carboxy and amino termini of cytochrome b_5 form an independent structural unit that can be monitored via NOE contacts. Even though α6 showed a dramatic decrease in α-helical content during the simulation, it remained docked to the carboxy terminus of this structural unit (Moore & Lecomte, 1990). β5 showed very low secondary structure content as well as a loss of interstrand contacts with β4 during one portion of the simulation. However, the NOE connectivities predicted from the simulation indicate that the carboxy end of β5 was at all times docked onto the loop between β3 and β4. The secondary structure content based on dihedral angles is particularly stringent and can misleadingly give the idea that some of the secondary structure was unstable, which is not borne out by the hydrogen bond and NOE analysis. Because of its sensitivity, however, this definition is useful for highlighting the dynamic behavior of the secondary structure. Overall, the simulation is in very good agreement with the data describing the solution structure of cytochrome b_5.

Although large average deviations from the crystal structure were observed during the simulation, the system was stable based on structural grounds and was at all times consistent with the solution NMR data. Such a long and stable trajectory is certainly encouraging in spite of, or maybe because of, the fact that large deviations are observed but drop with increasing simulation time. Thus, movement away from the crystal structure does not necessarily indicate that the protein is drifting in conformational space never to return. Optimistically, we may be sampling the relevant dynamical and structural properties of the equilibrium native state. But, as always, longer simulations are necessary to test this idea.

Nevertheless, whenever there are large movements away from the crystal structure in a simulation, the results must be carefully scrutinized. Generally, such deviations are taken as prima facie evidence that a simulation is unstable and it is then terminated. While this may be the case, several indirect pieces of evidence suggest that the motion exhibited by cytochrome b_5 may be real: (1) Even when the deviation from the crystalline conformation was large, the structures were consistent with the solution NMR data. (2) The motion was localized to three specific regions of the protein (residues 10−20, 40−52, and 65−75). Two of these regions (regions 1 and 2) exhibit increased motion in the crystal structure, although region 2 shows less motion than observed in the simulation. However, this region and region 3 appear to be involved in crystal contacts (Mathews et al., 1972), which may impair their motion. (3) Various NMR studies (Guiles et al., 1990, 1992; Mauk et al., 1986; McLachlan et al., 1988; Meyer et al., 1993; Reid et al., 1987; Veitch et al., 1988) indicate that the protein is more dynamic in solution than in the crystalline state. Furthermore, Veitch et al. (1990) found that residues 39−42 (region 2) are particularly mobile. (4) After deviating from the crystal structure, the crystalline conformation was restored and reached a C_α RMS deviation from the crystal structure that is better than has been obtained in many shorter simulations [<200 ps; see review by Daggett and Levitt (1993)]. Furthermore, the deviations from the crystal structure and regions of high mobility may be biologically relevant.

As mentioned above, three specific regions of the protein contributed when a large C_α RMS deviation from the crystal structure was observed. The first two regions are at the interface of core 1 and core 2 (Figure 1). The second region incorporates most of the acidic residues implicated in protein−protein interactions. Even though both regions were highly mobile, this motion was not correlated (data not presented). That is, as one increased, the other did not necessarily increase or decrease systematically. However, these backbone deviations translated into conformational changes on the surface of the protein. For example, the surface pattern displayed by the acidic residues in region 2 changed with time (Figure 5). In addition, a large cleft formed as a result of the main-chain motion, exposing several hydrophobic residues of core 1 (Figure 6). Furthermore, the periodic exposure of the core residues suggested a breathing motion of the protein.

A vast amount of experimental work has been performed attempting to reveal the mechanism of cytochrome b_5 protein−protein complex formation. Cytochrome b_5 interacts with a variety of proteins, including cytochrome b_5 reductase, cytochrome *c*, hemoglobin, and the cytochrome P-450s. Thus, this protein must discern and interact with a structurally varied set of proteins. Studies utilizing computer modeling, chemical modification, and mutagenesis have implicated some of the acidic residues as mediators of cytochrome b_5 complex formation.

On the basis of the pioneering work of Salemme (1976), a cytochrome b_5−cytochrome *c* complementary charge-paired complex was proposed and tested further (Wendoloski et al., 1987). In accord with these models, site-directed mutagenesis experiments coupled with high-pressure techniques suggest that Glu 44, Glu 48, Asp 60, and the heme propionate group are important in maintaining and/or forming this complex (Rodgers et al., 1988). On the other hand, other nearby residues (Gln 13, Glu 37, Glu 43, Glu 56, and Asp 66) are not involved (Rodgers & Sligar, 1991). In agreement with the findings of Rodgers et al. (1988), Whitford (1992) used 1- and 2-D NMR to show that Glu 44 and Glu 48 are involved in complex formation, in addition to Glu 37, Glu 38, and Glu 43. That Glu 37 and Glu 43 are implicated is in contrast to the findings of Rodgers and Sligar (1991). Strittmatter et al. (1990) characterized the cross-linking of a cytochrome b_5−cytochrome b_5 reductase complex and suggest that Glu 43, Glu 44, Glu 48, Glu 56, Asp 60, and the heme propionate are important in interfacial interactions. Although Glu 43 forms a salt bridge with Arg 47, constraining the mobility of these two residues, the other residues within this region are known to be quite mobile (Veitch et al., 1990).

The acidic residues mentioned above are conserved across all cytochrome b_5 forms to date with the exception of one conservative change, Glu 37 → Asp in chicken (Ozols, 1989). These residues belong to a region (residues 37−60) that is located along the periphery of the heme cavity. It has been proposed that the conformational flexibility of these residues could either provide long-range steering for initial complex formation (Matthew et al., 1983) or fine tune the orientation of the complex for maximal electron-transfer activity (Salemme, 1976). In any case, it is still unclear as to exactly

FIGURE 8: Stereo diagram of the C_α backbone of cytochrome b_5: crystal structure and 1.66 ns snapshot from the simulation. The acidic residues implicated in protein−protein recognition are shown with van der Waal's surfaces displayed. Site I on the left contains Glu 56 and Asp 60, and site II on the right consists of Glu 37, 38, 43, 44, and 48. Most studies of cytochrome b_5 complexes assume that the protein−protein interface spans both sites and the heme group as shown with the curved line. The arrow near the structure from the simulation (1.66 ns) indicates the position of the cleft.

which conformational displays of the acidic residues of cytochrome b_5 are responsible for interacting with other proteins. Furthermore, removal of Glu 44, Glu 48, and Asp 60 and modification of the heme propionate yields only a 14% decrease in free energy of association to cytochrome c (Rodgers & Sligar, 1991); this finding suggests that the electrostatic interactions implicated thus far only play a minor role in complex recognition/formation. However, specificity is not always linked to stability, and these interactions could still be important in obtaining favorable electron-transfer geometries. In any case, a hydrophobic patch, as revealed through the simulation, could provide an additional mode of interaction regulated by intermittent exposure to the solvent.

Most of the docking studies to date propose that the partially exposed heme groups of the interacting species in the complex are nearly coplanar with minimal separation between the heme edges, an arrangement that may be favorable for electron transfer (Poulos & Mauk, 1983; Salemme, 1976). Stayton et al. (1989), however, have suggested that the heme groups may be perpendicular in a cytochrome b_5−cytochrome P-450$_{cam}$ complex. In each case, acidic groups flanking both sides of the heme crevice appear to contribute to the complex interface (Figure 8). However, an alternative mode of interaction between cytochrome b_5 and cytochrome c has also been proposed. Hartshorn et al. (1987) found that a paramagnetic relaxation probe interacts with the exposed heme propionate of a complexed cytochrome b_5. This suggests that the propionate group is exposed and the alignment of the proteins has changed and does not involve the entire putative binding surface depicted in Figure 8. In addition, Whitford (1992) found that cytochrome c shields only one anionic patch of cytochrome b_5, involving Glu residues 37, 38, 43, 44, and 48, which fall on one side of the heme crevice (right-hand side of the protein, Figure 8). These findings suggest that although an electrostatic interaction does take place, it need not necessarily lead to a coplanar arrangement of the heme groups, as is suggested by the original Salemme (1976) model. In addition, the heme groups are not coplanar in the crystal structure of a cytochrome c−cytochrome c peroxidase complex; instead, they make an angle of ~60° to each other (Pelletier & Kraut, 1992).

The cleft identified in the simulation is near the main patch of acidic residues implicated in protein−protein contacts by all investigators (Figure 8). Because of the close proximity of the cleft to these acidic residues, it seems likely that it could contribute to recognition and binding, even assuming

the binding mode suggested by Salemme (see Figure 8). Alternatively, in another shifted binding mode, the position and depth of this cleft could allow the partner in the complex access to the heme group (Figure 8). Thus, our results suggest that another portion of the molecule, in addition to, or in lieu of, the binding surface indicated in Figure 8, may be important in recognition. And, as discussed by Cherfils et al. (1991), there can be several distinct solutions to the macromolecular recognition problem. In any case, if the heme portion of cytochrome b_5's partner were to bind within the cleft, one would not obtain a coplanar arrangement of heme groups. Docking of our 1.66 ns snapshot of cytochrome b_5 with the cytochrome *c* crystal structure reveals that it is possible to construct a complex whereby a hydrophobic patch near the heme group of cytochrome *c* fits into the cleft on cytochrome b_5 (data not shown). Furthermore, the acidic residues above the cleft (right-hand side of the protein, Figure 8) have salt-bridging partners on cytochrome *c* even in this orientation. We are currently refining this complex and constructing others utilizing different conformations adopted during the simulation in an attempt to more directly correlate the observed surface properties with the different interfacial interactions cytochrome b_5 must be involved in with different proteins. In addition, we are testing our hypothesis by making mutations aimed at perturbing cleft formation and seeing whether there is an effect on complex formation, utilizing both simulations and experimental techniques (Storch, Daggett, and Atkins, work in progress).

The ability to display different surfaces utilizing solely native thermal motion may represent a low-energy mechanism for controlling recognition processes. Over a decade ago, Tainer et al. (1984) demonstrated that mobility is a major factor in recognition of native proteins by antipeptide antibodies, and they speculated that it may be generally valid in protein−protein recognition. They suggested that proteins adopt a range of conformations and only bind to antibodies when a particular conformation recognized by the antibody is displayed. Furthermore, they note that the many conformations adopted in solution and displayed to the antibodies can differ from the average structure seen by X-ray crystallography. On the basis of our findings, we suggest that this may also be the case with cytochrome b_5. Thus, we could envision different conformations interacting with different proteins, and binding occurs when a favorable surface is displayed or the cleft, if involved, is accessible. Along these lines, many investigators have discussed the importance of flexibility in fine tuning interfacial interactions of electron-transfer protein complexes involving cytochrome b_5 (Burch et al., 1990; Mauk et al., 1986; Meyer et al., 1993; Wendoloski et al., 1987). Our findings would just take this a step further and suggest that flexibility may also be important in recognition prior to actual complex formation.

ACKNOWLEDGMENT

We thank Bill Atkins for interesting discussions and Pat Stayton for providing helpful comments on the manuscript. With the exception of Figure 1, the molecular graphics images were produced using the MidasPlus program from the Computer Graphics Laboratory, University of California, San Francisco (supported by NIH Grant RR-01081) (Ferrin et al., 1988; Huang et al., 1991).

REFERENCES

Altman, J., Lipka, J. J., Kuntz, I. D., & Waskell, L. (1989) *Biochemistry 28*, 7516−7523.
Braatz, J. A., Paulsen, M. D., & Ornstein, R. L. (1992) *J. Biomol. Struct. Dyn. 9*, 935−949.
Brunne, R. M., Liepinsh, E., Otting, G., Wüthrich, K., & van Gunsteren, W. F. (1993) *J. Mol. Biol. 231*, 1040−1048.
Burch, A. M., Rigby, S. E. J., Funk, W. D., MacGillivray, R. T. A., Mauk, M. R., Mauk, G., & Moore, G. R. (1990) *Science 247*, 831−833.
Careaga, C. L., & Falke, J. J. (1992) *J. Mol. Biol. 226*, 1219−1235.
Chandrasekhar, I., Clore, G. M., Szabo, A., Gronenborn, A. M., & Brooks, B. R. (1992) *J. Mol. Biol. 226*, 239−250.
Cherfils, J., Duquerroy, S., & Janin, J. (1991) *Proteins Struct., Funct., Genet. 11*, 271−280.
Clore, G. M., Gronenborn, A. M., James, M. N. G., Kjaer, M., McPhalen, C. A., & Poulsen, F. M. (1987) *Protein Eng. 1*, 313−318.
Daggett, V., & Levitt, M. (1992) *J. Mol. Biol. 223*, 1121−1138.
Daggett, V., & Levitt, M. (1993) *Annu. Rev. Biophys. Biomol. Struct. 22*, 353−380.
Daggett, V., Kollman, P. A., & Kuntz, I. D. (1991) *Biopolymers 31*, 1115−1134.
Ferrin, T. E., Huang, C. C., Jarvis, L. E., & Langridge, R. (1988) *J. Mol. Graphics 6*, 13−27.
Guiles, R. D., Altman, J., Kuntz, I. D., & Waskell, L. (1990) *Biochemistry 29*, 1276−1289.
Guiles, R. D., Basus, V. J., Kuntz, I. D., & Waskell, L. (1992) *Biochemistry 31*, 11365−11375.
Hartshorn, R. T., Mauk, A. G., Mauk, M. R., & Moore, G. R. (1987) *FEBS Lett. 213*, 391−395.
Hegesh, E., Hegesh, J., & Kaftory, A. (1986) *N. Engl. J. Med. 314*, 757−761.
Henry, E. R., Levitt, M., & Eaton, W. A. (1985) *Proc. Natl. Acad. Sci. U.S.A. 82*, 2034−2038.
Hong, M. K., Braunstein, D., Cowen, B. R., Frauenfelder, H., Iben, I. E. T., Mourant, J. R., Ormos, P., Scholl, R., Schulte, A., Steinback, P. J., Xie, A., & Young, R. D. (1990) *Biophys. J. 58*, 429−436.
Housset, D., Kim, K., Fuchs, J., Woodward, C., & Wlodawer, A. (1991) *J. Mol. Biol. 220*, 757−770.
Hua, Q., & Weiss, M. A. (1990) *Biochemistry 29*, 10545−10555.
Huang, C. C., Pettersen, E. F., Klein, T. E., Ferrin, T. E., & Langridge, R. (1991) *J. Mol. Graphics 9*, 230−236.
Kabsch, W. (1976) *Acta Crystallogr., Sect. A 32*, 922−923.
Kell, G. S. (1967) *J. Chem. Eng. Data 12*, 66−69.
Kline, A. D., Braun, W., & Wüthrich, K. (1988) *J. Mol. Biol. 204*, 675−685.
Kraulis, P. (1991) *J. Appl. Crystallogr. 24*, 946−950.
Lecomte, J. T. J., & Moore, C. D. (1991) *J. Am. Chem. Soc. 113*, 9663−9665.
Lederer, F., Ghrir, R., Guiard, B., Cortial, S., & Ito, A. (1983) *Eur. J. Biochem. 132*, 95−102.
Lee, B., & Richards, F. M. (1971) *J. Mol. Biol. 55*, 379−400.
Levitt, M. (1983) *J. Mol. Biol. 168*, 595−620.
Levitt, M. (1989) *Chem. Scr. 29A*, 197−203.
Levitt, M. (1990) *ENCAD-Energy Calculation and Dynamics*, Molecular Applications Group, Palo Alto, CA.
Levitt, M., Hirshberg, M., Sharon, R., & Daggett, V. (1995a) *Comput. Phys. Commun.* (in press).
Levitt, M., Hirshberg, M., Sharon, R., & Daggett, V. (1995b) (submitted for publication).
Li, A., & Daggett, V. (1995) (submitted for publication).
Livingston, D. J., McLachlan, S. J., La Mar, G. N., & Brown, W. D. (1985) *J. Biol. Chem. 260*, 15699−15707.
Mathews, F. S., & Czerwinski, E. W. (1976) in *The Enzymes of Biological Membranes* (Martonosi, A., Ed.) Vol. 4, pp 143−198, Plenum Press, New York.
Mathews, F. S., Argos, P., & Levine, M. (1972) *Cold Spring Harbor Symp. Quant. Biol. 36*, 387−395.
Mathews, F. S., Czerwinski, E. W., & Argos, P. (1979) in *The Porphyrins* (Dolphin, D., Ed.) Vol. VII, Part B, pp 123−125, Academic Press, Inc., New York.

Matthew, J. B., Weber, P. C., Salemme, F. R., & Richards, F. M. (1983) *Nature 301*, 169−171.
Mauk, M. R., & Mauk, A. G. (1989) *Eur. J. Biochem. 186*, 473−486.
Mauk, M. R., Mauk, A. G., Weber, P. C., & Matthew, J. B. (1986) *Biochemistry 25*, 7085−7091.
McLachlan, S. J., La Mar, G. N., & Lee, K. B. (1988) *Biochim. Biophys. Acta 957*, 430−445.
Meyer, T. E., Rivera, M., Walker, F. A., Mauk, M. R., Mauk, A. G., Cusanovich, M. A., & Tollin, G. (1993) *Biochemistry 32*, 622−627.
Moore, C. D., & Lecomte, J. T. J. (1990) *Biochemistry 29*, 1984−1989.
Moore, C. D., & Lecomte, J. T. J. (1993) *Biochemistry 32*, 199−207.
Moore, C. D., Ousaima, N. A., & Lecomte, J. T. J. (1991) *Biochemistry 30*, 8357−8365.
Ng, S., Smith, M. B., Smith, H. T., & Millet, F. (1977) *Biochemistry 16*, 4975−4978.
Ozols, J. (1989) *Biochim. Biophys. Acta 997*, 121−130.
Pelletier, H., & Kraut, J. (1992) *Science 258*, 1748−1755.
Pflugrath, J. W., Wiegand, G., Huber, R., & V'ertesy, L. (1986) *J. Mol. Biol. 189*, 383−392.
Poulos, T. L., & Mauk, A. G. (1983) *J. Biol. Chem. 258*, 7369−7373.
Reid, L. S., Gray, H. B., Dalvit, C., Wright, P. E., & Saltman, P. (1987) *Biochemistry 26*, 7102−7107.
Rodgers, K. K., & Sligar, S. G. (1991) *J. Mol. Biol. 221*, 1453−1460.
Rodgers, K. K., Pochapsky, T. C., & Sligar, S. G. (1988) *Science 240*, 1657−1659.
Salemme, F. R. (1976) *J. Mol. Biol. 102*, 563−568.
Schenkman, J. B., & Greim, H. (1993) in *Cytochrome P450*, pp 147−150, Springer-Verlag, Berlin.
Smith, J. L., Hendrickson, W. A., Honzatko, R. B., & Sheriff, S. (1986) *Biochemistry 25*, 5018−5027.
Stayton, P. S., Poulos, T. L., & Sligar, S. G. (1989) *Biochemistry 28*, 8201−8205.
Strittmatter, P., & Velick, S. F. (1956) *J. Biol. Chem. 221*, 253−264.
Strittmatter, P., Hacket, C. S., Korza, G., & Ozols, J. J. (1990) *J. Biol. Chem. 265*, 21709−21713.
Tainer, J. A., Getzoff, E. D., Alexander, H., Houghten, R. A., Olson, A. J., Lerner R. A., & Hendrickson, W. A. (1984) *Nature 312*, 127−134.
Tamburini, P. P., White, R. E., & Schenkman, J. B. (1985) *J. Biol. Chem. 260*, 4007−4015.
Urbanova, M., Dukor, R. K., Pancoska, P., Gupta, V. P., & Keiderling, T. A. (1991) *Biochemistry 30*, 10479−10485.
Veitch, N. C., Concar, D. W., Williams, R. J., & Whitford, D. (1988) *FEBS Lett. 238*, 49−55.
Veitch, N. C., Whitford, D., & Williams, R. J. P. (1990) *FEBS Lett. 269*, 297−304.
Weiss, M. A., Nguyen, D. T., Khait, I., Inouye, K., Frank, B. H., Beckage, M., O'Shea, E., Shoelson, S. E., Karplus, M., & Neuringer, L. J. (1989) *Biochemistry 28*, 9855−9873.
Wendoloski, J. J., Matthew, J. B., Weber, P. C., & Salemme, F. R. (1987) *Science 238*, 794−797.
Whitford, D. (1992) *Eur. J. Biochem. 203*, 211−223.
Wittekind, M., Rajagopal, P., Branchini, B. R., Reizer, J., Saier, M. H., Jr., & Klevit, R. E. (1992) *Protein Sci. 1*, 1363−1376.
Wüthrich, K., Ed. (1986) in *NMR of Proteins and Nucleic Acids*, pp 111−113, John Wiley & Sons, Inc., New York.

BI9503763